Preparation and Properties of Polyimide–Clay Nanocomposite Materials for Anticorrosion Application

Yuan-Hsiang Yu,[1,2] Jui-Ming Yeh,[1] Shir-Joe Liou,[1] Chi-Lun Chen,[1] Der-Jang Liaw,[3] Hsin-Yi Lu[3]

[1]*Department of Chemistry and Center for Nanotechnology at CYCU, Chung-Yuan Christian University, Chung Li 320, Taiwan, Republic of China*
[2]*Department of Electronic Engineering, Lan-Yan Institute of Technology, I-Lan 261, Taiwan, Republic of China*
[3]*Department of Chemical Engineering, National Taiwan University of Science and Technology, Taipei 106, Taiwan, Republic of China*

Received 8 July 2003; accepted 2 December 2003

ABSTRACT: A series of polymer–clay nanocomposite (PCN) materials that consist of organosoluble polyimide and layered montmorillonite clay were prepared by the solution dispersion technique. The organosoluble polyimide containing non-coplanar moiety in diamine monomer and flexible bridging linkages in dianhydride monomer was synthesized by chemical imidization. The as-synthesized PCN materials were characterized by infrared spectroscopy, wide-angle powder X-ray diffraction, and transmission electron microscopy. The organosoluble polyimide showed better corrosion resistance compared to polyaniline, poly(*o*-ethoxyaniline) and poly(methyl methacrylate) by using a series of standard electrochemical corrosion measurements of corrosion potential, polarization resistance, and corrosion current in 5 wt % aqueous NaCl electrolyte. Polyimide–clay nanocomposite materials incorporated with low loading of clay were found to further improve corrosion inhibition over pure polyimide. Effects of the material composition on the O_2/H_2O molecular permeability, optical clarity, and thermal properties of polyimide–clay nanocomposite materials were studied by molecular permeability analysis, UV–visible transmission spectra, thermogravimetric analysis, and differential scanning calorimetry, respectively. © 2004 Wiley Periodicals, Inc. J Appl Polym Sci 92: 3573–3582, 2004

Key words: polyimide; clay; nanocomposite; anticorrosion

INTRODUCTION

Aromatic polyimides were thermally stable polymers that exhibit excellent mechanical strength and thermal stability. During the past decades, research interest in these polymers increased corresponding to the increasing technological applications in a variety of fields such as aerospace, automobile, and microelectronics. Recently, significant synthetic efforts in the research field of aromatic polyimides had focused on enhancing the solubility through a variety of structural modifications of new diamine or dianhydride monomers. Several approaches for the preparation of soluble polyimides such as the incorporating of flexible bridging linkages,[1,2] bulky substituents,[3,4] non-coplanar conformation units,[5,6] as well as pendent groups[7,8] into polymer backbone led to significant success.

The historical development of the polymer–clay nanocomposite (PCN) materials could be traced back to 1990 based on the research work of polyamide–clay nanocomposite by Toyota's research group.[9] The montmorillonite (MMT) clay consisted of two fused tetrahedral silica sheets sandwiching an edge-shared octahedral sheet of either magnesium or aluminum hydroxide. Organic treatment of the layered MMT was required for compatibility with most polymers. For example, the Na^+ and Ca^{2+} existing in the interlayer regions could be replaced by organic cations such as alkylammonium ions through a cationic-exchange reaction to render the hydrophilic layer silicate organophilic, leading to the striking development of PCN materials. Based on much published literature, the dispersion of nanolayers of mineral clay was reported to improve the thermal stability,[10] mechanical strength,[11] molecular barrier,[12] and flame resistance[13] properties of polymers.

Lately, there was a considerable amount of publications associated with the preparation and properties of polyimide–clay nanocomposite[14–18] and organosoluble polyimide–clay nanocomposite materials.[19–22] However, there were no practical coating applications for these various structurally modified soluble polyimide–clay nanocomposite materials.

Many novel coating materials with effective anticorrosion properties attracted considerable research attention in recent decades.[23–28] The use of polymeric coatings to protect metals against corrosion had been employed for a long time. In general, the primary effect of a polymeric coating was to function as a

Correspondence to: J.-M. Yeh (juiming@cycu.edu.tw).
Contract grant sponsor: NSC; contract grant number: 90-2113M-033-010.

physical barrier against aggressive species such as O_2 and H^+. Recently, we demonstrated the corrosion inhibition effect of pristine polymers [e.g., polyaniline (PANI),[29,30] poly(methyl methacrylate) (PMMA)[31]] can be effectively enhanced by incorporating the inorganic nanolayers of MMT clay into the organic polymeric matrix based on a series of electrochemical corrosion measurements on PCN materials coated on cold-rolled steel (CRS) coupon.

In this article, the incorporation of both non-coplanar 2,2′-disubstituted biphenylene and flexible aryl ether units into the polymer backbone was designed to improve solubility for coating application. We found that this non-coplanar soluble polyimide (NSPI) showed better corrosion resistance compared to PANI, poly(*o*-ethoxyaniline) (PEA), and PMMA by using a series of standard electrochemical corrosion measurements. A series of NSPI–clay nanocomposite materials in the form of coating had applied for the corrosion protection on metallic surface and was shown to be superior in anticorrosion over pure NSPI. The as-synthesized PCN materials were characterized by wide-angle powder X-ray diffraction, transmission electron microscopy (TEM), and infrared spectroscopy. The effect of material composition on the molecular barrier, optical clarity, and thermal properties were also studied by the molecular permeability analysis, UV–visible transmission spectra, differential scanning calorimetry (DSC), and thermogravimetric analysis (TGA), respectively.

EXPERIMENTAL

Chemicals and instrumentations

2,2-Bis[4-(dicarboxyphenoxy)phenyl]propane dianhydride (Shanghai Research Institute of Synthetic Resin, China), *N*,*N*-dimethylacetamide (DMAc; Mallinckrodt, Paris, KY), pyridine (Riedel-de Haën), acetic anhydride (Fisher Chemical, New Jersey), *N*-methyl-2-pyrrolidinone (NMP; Tedia, 99.97%, Fairfield, CT), tetrahydrofuran (THF; 99%, Merck, Darmstadt, Germany), *N*,*N*-dimethylformamide (DMF; Fluka, Buchs, Switzerland), *m*-cresol (Fluka), and methanol (Riedel-deHaën) were used as received without further purification. 2,2′-Dimethyl-4,4′-bis(aminophenoxy)biphenyl was synthesized according to the procedure of Liaw et al.[5] HCl (1.0*M*) was prepared from hydrochloric acid (Riedel-deHaën) with distilled water for preparing the acidic media. (4-Carboxybutyl)-triphenylphosphosphonium bromide (Lancaster, 98%) was used as intercalating agent. The used montmorillonite clay consisted of a unit cell formula $[Na_{0.48}K_{0.01}Ca_{0.01}Ti_{0.01}](Fe_{0.20}Al_{1.44}Mg_{0.31})(Si_{3.39}Al_{0.07})O_{10}(OH)_2{\cdot}2H_2O$ and a CEC value of 98 meq/100 g provided by Pai-Kong Ceramic Co. (Taiwan, China).

FTIR spectra were measured on pressed KBr pellets by using a Jasco FTIR-460 plus spectrometer. Wide-angle X-ray diffraction study of the samples was performed on a Rigaku D/MAX-3C OD-2988N X-ray diffractometer with a copper target and Ni filter at a scanning rate of 4°/min. The samples for TEM study were first prepared by putting the membrane of PCN materials into epoxy resin capsules followed by curing the epoxy resin at 100°C for 24 h in a vacuum oven. Then the cured epoxy resin containing PCN materials were microtomed with a Reichert-Jumg Ultracut-E into 60- to 90-nm-thick slices. Subsequently, one layer of carbon about 10 nm thick was deposited on these slices on mesh-100 copper nets for TEM observations on a JEOL-200FX with an acceleration voltage of 120 kV.

Electrochemical measurements of corrosion potential, polarization resistance, and corrosion current on sample-coated CRS coupons were performed on VoltaLab 21 Potentiostat/Galvanostat in a standard corrosion cell equipped with two graphite rod counterelectrodes and a saturated calomel electrode (SCE) as well as the working electrode. A Yanagimoto Co., Ltd. gas permeability analyzer (model GTR 10) was employed to perform the permeation experiment of oxygen gas and water vapor. UV–visible transmission spectra were obtained by using a Hitachi U-2000 UV–Vis spectrometer. Perkin–Elmer Thermal Analysis System equipped with model 7/DX TGA was employed to perform the thermal analyses from 50 to 800°C temperature range at a heating rate of 20°C/min under airflow. DSC was performed on a Perkin–Elmer model 7 DSC analyzer in the 130–240°C range at the programmed heating rate of 10°C/min. The molecular weight of NSPI was determined on a Waters GPC model 2 II equipped with a model 590 programmable solvent delivery module, a differential refractometer detector, and a Styragel HT column with THF as eluant and monodispersed polystyrenes as calibration standards.

Preparation of non-coplanar soluble polyimide (NSPI) by chemical imidization

A representative step to synthesize NSPI through chemical imidization was given as follows: 2,2-bis-[4-(dicarboxyphenoxy)phenyl]propane dianhydride (1.56 g, 3 mmol) in DMAc (12 g) was gradually added to a stirred solution of 2,2′-dimethyl-4,4′-bis(aminophenoxy)biphenyl (1.188 g, 3 mmol) in DMAc (12 g). The mixture was magnetically stirred for 24 h at room temperature to form the poly(amic acid). An equimolar mixture of acetic anhydride (0.612 g, 6 mmol) and pyridine (0.48 g, 6 mmol) was added into the prepared poly(amic acid) solution. The mixture was stirred at room temperature for 1 h and then heated at 100°C for 2 h. Methanol (300 mL) was then poured into the solution and the solid precipitate was subsequently filtered off, washed with hot water and methanol, and then dried under vacuum to afford NSPI with a

weight-average molecular weight of 148,191 g/mol. Yield was more than 90%.

Preparation of organophilic clay

The organophilic clay was prepared by a cationic-exchange reaction between the sodium cations of MMT clay and quaternary alkylphosphonium cations of (4-carboxybutyl)-triphenylphosphosphonium bromide. The equation to calculate the used intercalating agent amount for cationic-exchange reaction was

$$98/100 \times 5 \text{ g (for clay)} \times 1.2 = (X/M_w \text{of intercalating agent}) \times 1 \times 1000$$

where X is the amount of used intercalating agent, 98/100 represents the cationic exchange capacity (CEC) value per 100 g MMT clay, and 1.2 (>1) indicates that the excess amount of intercalating agent was used. Typically, 5 g MMT clay with a CEC value of 98 meq/100 g was stirred in 400 mL distilled water (beaker A) at room temperature overnight. A separate solution contains an excess amount of intercalating agent (2.52 g) in another 30 mL of distilled water (beaker B) under magnetic stirring, follow by adding 1*M* HCl aqueous solution to adjust the pH value to about 3–4. After stirring for 1 h, the solution containing an excess amount of intercalating agent (beaker B) was added at a rate of ~ 10 mL/min with vigorous stirring to the MMT suspension (beaker A). The mixture was stirred overnight at room temperature. The organophilic clay was recovered by ultracentrifuging (9000 rpm, 30 min). Product purification could be performed through washing and ultracentrifuging samples repeatedly for at least three times to remove any excess of intercalating agent.

Preparation of NSPI–clay nanocomposite materials

NSPI–clay nanocomposite materials were prepared by the solution dispersion technique. First, organophilic clay content calculated by 0.5, 1, 3, and 5 wt % with respect to NSPI was introduced into NMP under magnetic stirring 24 h at room temperature. Six weight percent solutions of PCN materials in NMP were prepared by the addition of NSPI into each of the dispersed organophilic clay solutions. Under magnetic stirring for an additional 12 h at room temperature, excess methanol was poured into the as-prepared PCN solution. Filtering, washing with hot water and methanol, and then drying under vacuum at 40°C resulted in the NSPI–clay nanocomposite materials for further preparation of coatings onto CRS coupons for electrochemical measurements.

Following is an example of 6 wt % solution of PCN materials containing 1 wt % organophilic clay: 0.0084 g organophilic clay was dispersed in 13.16 g of NMP under magnetic stirring for 24 h at room temperature. The PCN solution was prepared by introducing 0.8316 g of NSPI into organophilic clay solution and further stirring for 12 h at room temperature.

Preparation of coatings and electrochemical measurements

Six weight percent solutions of NSPI and PCN materials in NMP were filtered through a 0.45-μm hydrophilic PVDF filter (Millpore Millev-HV). Two drops of each solution were cast onto CRS coupons (1.0 × 1.0 cm). The coating was dried slowly in air for more than 48 h at 100°C on a hot plate to make sure the film was free of solvent to form ~ 20-μm-thick coating, measured by a digimatic micrometer (Mitutoyo). The coating ability of PCN on CRS was found similar to that of NSPI. The coated and uncoated coupons were then mounted to the working electrode so that only the coated side of the coupon was in direct contact with the electrolyte. The edges of the coupons were sealed with superfast epoxy cement (SPAR®). All the electrochemical measurements of corrosion potential, polarization resistance, and corrosion current were performed on a VoltaLab model 21 Potentiostat/Galvanostat and repeated at least three times. The electrolyte was NaCl (5 wt %) aqueous solution. The open circuit potential (OCP) at the equilibrium state of the system was recorded as the corrosion potential (E_{corr} in V versus SCE). The polarization resistance (R_p in Ω/cm^2) was measured by sweeping the applied potential from 20 mV below to 20 mV above the E_{corr} at a scan rate of 500 mV/min and recording the corresponding current change. The R_p value was obtained from the slope of the potential current plot. The Tafel plots were obtained by scanning potential from 250 mV below to 250 mV above the E_{corr} at a scan rate of 500 mV/min. Corrosion current (i_{corr}) was determined by superimposing a straight line along the linear portion of the cathodic or anodic curve and extrapolating it through E_{corr}. The corrosion rate (R_{corr}, in milli-inches per year, MPY) was calculated from

$$R_{corr} \text{ (MPY)} = [0.13\, i_{corr}\text{(E.W.)}]/[Ad]$$

where E.W. is the equivalent weight (in g/eq.), A is the area (in cm^2), and d is the density (in g/cm^3).

Preparation of membranes and barrier property measurements

Membranes of NSPI and PCN materials were cast from as-prepared NMP solutions onto glass plates (5 × 5 cm, ~ 3 mL/pcs). The solution concentration was 6 wt % and filtered through a 0.45-μm pore-size filter (Millpore Millev-HV). The membranes were dried in an oven at 100°C for 8 h. The films were lifted from the

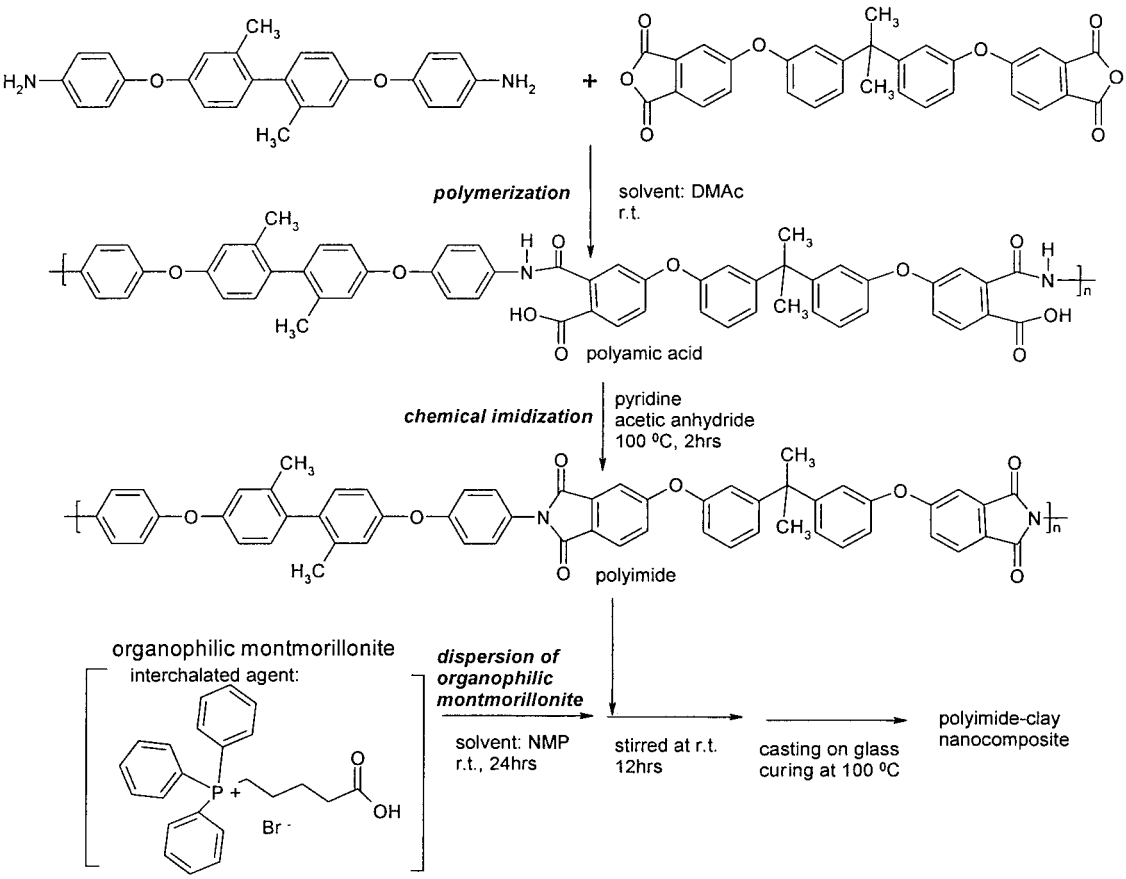

Scheme 1

glass plate by soaking in water to give membranes with thicknesses of ca. ~ 55 μm, measured by digimatic micrometer (Mitutoyo).

Oxygen permeability of membrane was determined by using the Yanco GTR-10 gas permeability analyzer. Gas permeability was calculated by

$$P = l/(p_1 - p_2) \times \frac{q/t}{A}$$

where P is the gas permeability [cm^3(STP)-cm/cm^2-s-cmHg], q/t is the volumetric flow rate of gas permeate [cm^3(STP)/s], l is the membrane thickness [cm], A is the effective membrane area [cm^2], and p_1, p_2 are the pressures (cmHg) on the high-pressure and low-pressure sides of the membrane, respectively. The rate of transmission of O_2 was obtained by gas chromatography, from which the air permeability was calculated. Water-vapor permeation measurements were obtained by using the same apparatus as pervaporation, except that the feed solution was not in contact with the membrane. The feed solution was vaporized first and subsequently permeated through the membrane with an effective area of ~ 10.2 cm^2. The permeation rate was determined by measuring the weight of permeate.

RESULTS AND DISCUSSION

For studies in coating application, the solubility of polyimide had to be improved. The structure of polyimide should be designed to be flexible. A non-coplanar diamine monomer containing 2,2′-disubstituted biphenylene and a flexible dianhydride monomer containing a long backbone of aryl ether units were introduced to the polyimide. The preparation flowchart of the NSPI and PCN materials are shown as Scheme 1. NSPI was prepared by a two-step method of chemical imidization by using a non-coplanar diamine monomer 2,2′-dimethyl-4,4′-bis(aminophenoxy)-biphenyl and a flexible bridging dianhydride monomer 2,2-bis[4-(dicarboxyphenoxy)phenyl]propane dianhydride. The chemical conversion from poly(amic acid) to NSPI was carried out through the incorporation of pyridine and acetic anhydride into the poly(amic acid) solution and followed by heating the mixture up to 100°C. The organophilic clay was then dispersed into the NSPI matrix by the solution dispersion technique. For better film-coating formation, molecular weight and imidization process of NSPI were important. Molecular weight of NSPI was determined by gel permeation chromatography (GPC) with THF as eluant. High molecular weight (M_w = 148,191

TABLE I
Relations of the Composition of Noncoplanar Soluble Polyimide (NSPI)–MMT Clay Nonocomposite Materials with the E_{corr} R_p, i_{corr}, and R_{corr} Measured from Electrochemical Methods and Thermal Analysis by TGA

	Feed composition (wt %)		Electrochemical corrosion measurements[a]					Thermal analyses[c]	
Compound code	Polymer	MMT	E_{corr} (mV)	R_p (KΩ cm^2)	i_{corr} (nA/cm^2)	R_{corr} (MPY)	Thickness[b] (μm)	T_d (°C)	Char yield (wt %)
Bare	—	—	−604	2.7	1.9×10^4	36.7	—	—	—
NSPI	100	0	−401	2.4×10^2	69	1.3×10^{-1}	~ 20	517.1	0
NSPI-0.5%	99.5	0.5	−365	2.2×10^3	32	6.2×10^{-2}	~ 20	526.9	0.6
NSPI-1%	99	1	−265	3.8×10^3	22	4.2×10^{-2}	~ 20	527.3	2.2
NSPI-3%	97	3	−94	1.1×10^4	15	2.9×10^{-2}	~ 20	527.5	2.9
NSPI-5%	95	5	—	—	—	—	~ 20	529.2	4.7
PANI[29]	100	0	−590	3.4	1.2×10^4	23.3	~ 20	—	—
PEA[30]	100	0	−563	3.11	1.0×10^4	19.3	~ 20	—	—
PMMA[31]	100	0	−485	3.2×10^2	1.2×10^2	2.3×10^{-1}	~ 110	—	—

[a] Saturated calomel electrode was employed as reference electrode.
[b] As determined by digimatic micrometer.
[c] As determined from TGA measurements.

g/mol) of as-prepared NSPI was used for further NSPI–clay nanocomposite materials preparation. The solubility of these NSPI–clay nanocomposite materials was also related to the imidization process. Thermal imidization failed to apply for corrosion study because insoluble polyimide was prepared. NSPI and NSPI–clay nanocomposite materials that were prepared by chemical imidization were soluble in a variety of solvents, including NMP, DMAc, DMF, *m*-cresol, and THF. For the coating of electrochemical measurements on the CRS coupons, NMP was more suitable for corrosion studies than other solvents because film quality of NMP-based NSPI was better in our experiment. Other solvents resulted in poor transparency for coating film on CRS coupons. The composition of the PCN materials was varied from 0 to 5 wt % of clay with respect to NSPI content as summarized in Table I.

Characterization

Typical FTIR spectra of poly(amic acid) and NSPI prepared from chemical imidization were shown in Figure 1. FTIR spectroscopy confirmed the formation of poly(amic acid). As shown in Figure 1(a), the characteristic absorption bands of the amic acid[32] appeared near 3466 (N—H and O—H stretching), 1722 (acid, C═O stretching), 1600 (amide, C═O stretching), and 1511 cm^{-1} (N—H bending). The FTIR spectrum of NSPI conversed from poly(amic acid) is shown in Figure 1(b). The characteristic absorption bands of the imide ring[32] appeared near 1777 (asymmetric C═O stretching), 1722 (symmetric C═O stretching), 1377 (C—N stretching), and 744 cm^{-1} (imide ring deformation). Furthermore, the representative FTIR spectra of the organophilic clay in PCN materials are shown in Figure 2. Characteristic vibration bands

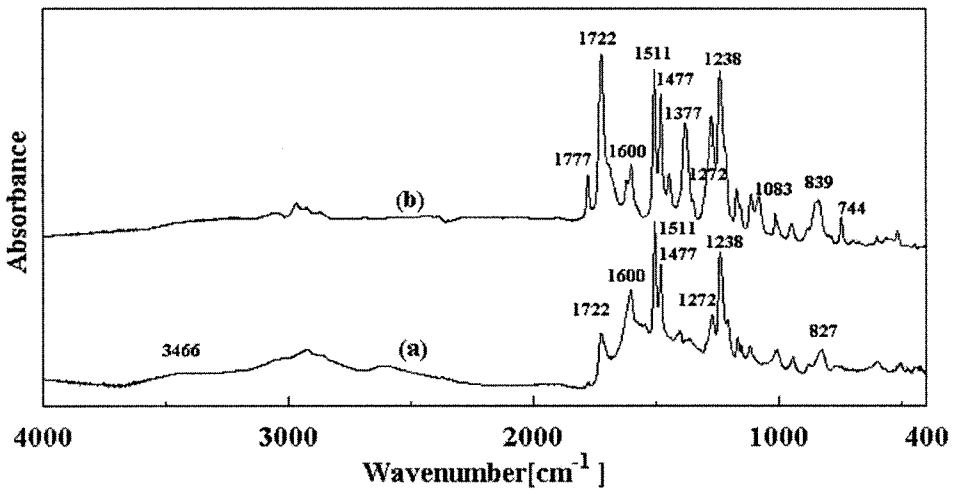

Figure 1 Representative FTIR spectra of (a) poly(amic acid), (b) non-coplanar soluble polyimide.

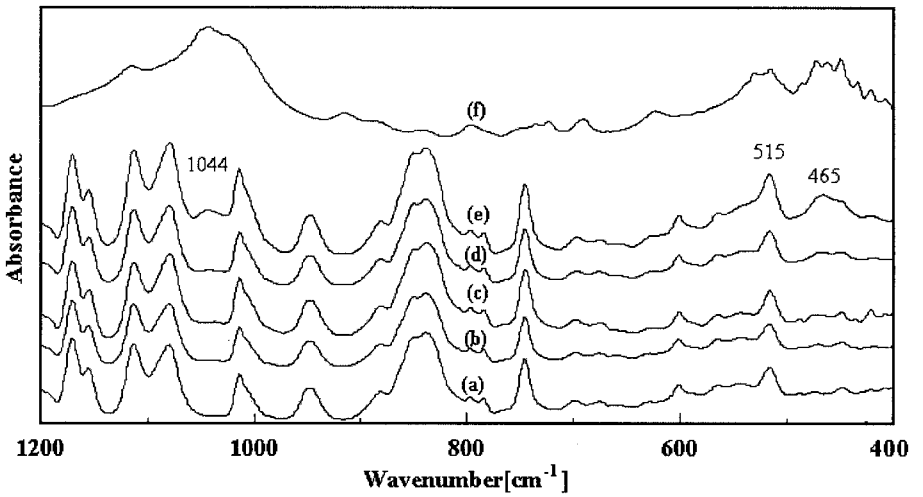

Figure 2 The FTIR spectra of (a) NSPI, (b) NSPI-0.5%, (c) NSPI-1%, (d) NSPI-3%, (e) NSPI-5%, (f) organophilic clay.

of MMT clay were shown at 1044 cm^{-1} (Si—O), 515 cm^{-1} (Al—O), and 465 cm^{-1} (Mg—O).[29–31] As the loading of organophilic MMT clay was increased, the intensities of organophilic MMT clay bands became stronger in the FTIR spectra of PCN materials.

Figure 3 shows the wide-angle powder X-ray diffraction patterns of organophilic clay, NSPI, and a series of PCN materials. For NSPI-1%, there was a lack of any diffraction peak in $2\theta = 2$–$10°$ as opposed to the diffraction peak at $2\theta = 5.15°$ (d-spacing = 17.1 Å) for organophilic clay, indicating the possibility of having exfoliated silicate nanolayers of organophilic clay dispersed in NSPI matrix. When the amount of clay increased up to 5 wt %, there was a small peak appearing at $2\theta = 4.5°$, corresponding to a d-spacing of 20.0 Å. This implies that some of organophilic clay could not exfoliate in NSPI and existed in the form of an intercalated layer structure. This result was further reconfirmed by visual observation from the TEM.

In Figure 4(a), the TEM image of PCN material with 1 wt % clay loading (i.e., NSPI-1%) primarily exhibited exfoliated morphology, which was consistent with the previous observation of powder X-ray diffraction patterns on as-prepared samples. Furthermore, in Figure 4(b), the TEM image of PCN material incorporated with 5 wt % clay showed that the lamellar nanocom-

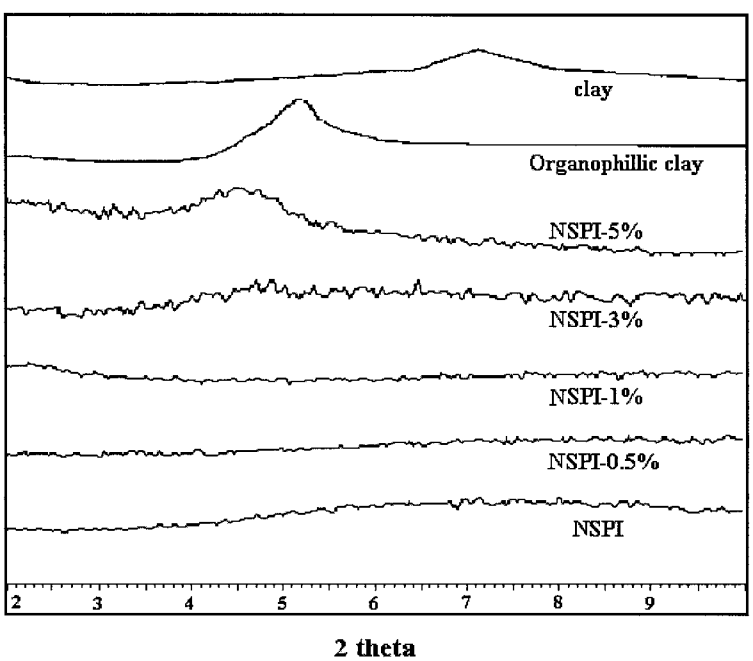

Figure 3 Wide-angle powder X-ray diffraction patterns of organophilic clay, NSPI, and a series of soluble PCN materials.

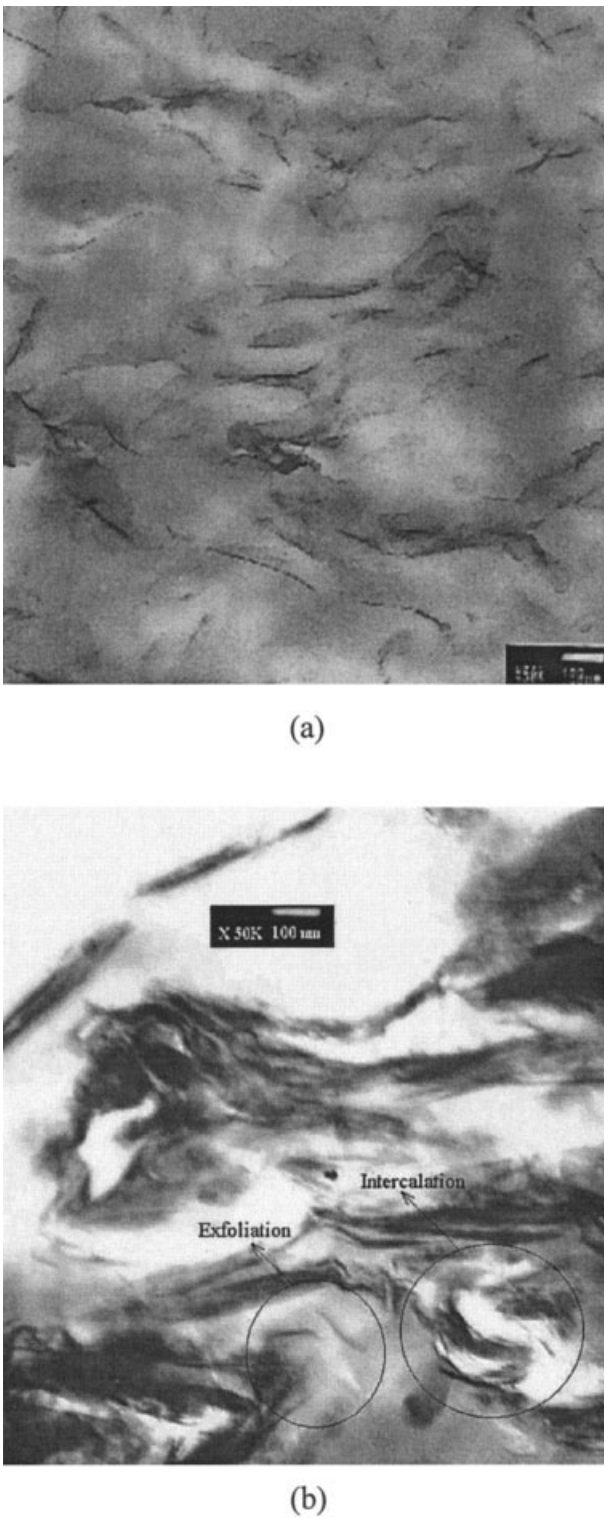

Figure 4 Transmission electron microscopy of (a) NSPI-1%, (b) NSPI-5%.

posite had a mixed nanomorphology. Individual silicate layers, along with two- and three-layer stacks, exfoliated in the NSPI matrix. Besides, some larger intercalated tactoids could also be identified.

Anticorrosive performance of coatings

Anticorrosive performance of sample-coated CRS coupons was evaluated from the values of corrosion potential (E_{corr}), polarization resistance (R_p), corrosion current (i_{corr}), and corrosion rate (R_{corr}), as listed in Table I. The CRS coupons coated with NSPI showed higher values in E_{corr} (−401 mV) and R_p (2.4×10^2 KΩ cm^2), and lower values in i_{corr} (69 nA/cm^2) and R_{corr} (0.13 milli-inches/year) than the uncoated CRS (E_{corr} = −604 mV, R_p = 2.7 KΩ cm^2, i_{corr} = 1.9×10^4 nA/cm^2, and R_{corr} = 36.7 milli-inches/year). This significant improvement in corrosion inhibition was associated with the effect of a polymeric coating functioning as a physical barrier against aggressive species. As compared to our previous publication, NSPI showed better corrosion resistance compared to PANI,[29] PEA,[30] and PMMA,[31] as listed in Table I. The corrosion rate for NSPI on CRS was 0.13 milli-inches/year that was vastly better than PEA (19.3 milli-inches/year) or PANI (23.3 milli-inches/year) in ~ 20-μm-thick coating. NSPI also showed a better corrosion rate on CRS than PMMA (0.23 milli-inches/year) even though the coating thickness of NSPI (~ 20 μm) was so thin as compared to PMMA (~ 110 μm). The corrosion current of NSPI was significantly enhanced in value to only 69 nA/cm^2, which was a small value to measure and about two orders of magnitude less than the uncoated CRS, which just used an ~ 20-μm coating. In our experience, if the thickness of NSPI coating was more than 50 μm, the data could not be detected in electrochemical corrosion measurements because the anticorrosion effect was too good to be measured.

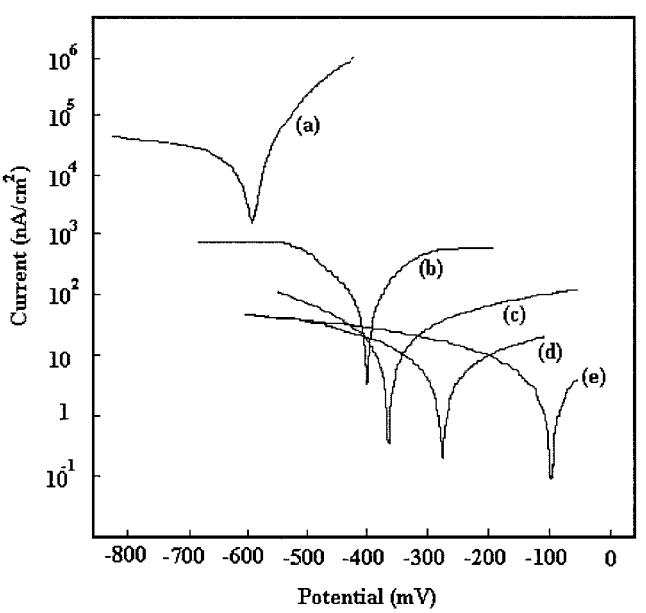

Figure 5 Tafel Plots for (a) uncoated, (b) NSPI-coated, (c) NSPI-0.5%-coated, (d) NSPI-1%-coated, (e) NSPI-3%-coated CRS measured in 5 wt % NaCl aqueous solution.

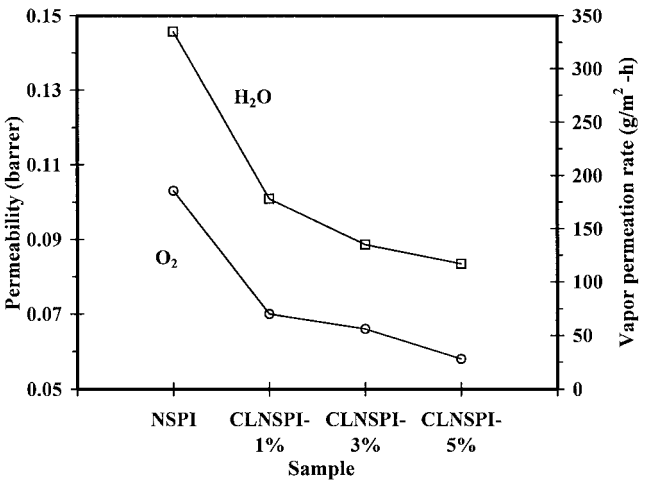

Figure 6 Permeability of O_2 and H_2O as a function of the MMT clay content in the NSPI–clay nanocomposite materials.

These reflected that NSPI might have significant potential for anticorrosion application. Furthermore, the anticorrosion performance increased along with the amount of organophilic clay dispersed in PCN materials. For example, the NSPI-3%-coated CRS had a higher corrosion potential of approximately −94 mV at 30 min. The polarization resistance (R_p) value of NSPI-3%-coated CRS was $\sim 1.1 \times 10^4$ kΩ/cm^2, which was more than three orders of magnitude as compared to the uncoated CRS. The corrosion current (i_{corr}) of NSPI-3%-coated CRS was only 15 nA/cm^2, which corresponded to a corrosion rate (R_{corr}) of $\sim 2.9 \times 10^{-2}$ milli-inches/year. These implied that the NSPI-3%-coated CRS was noble toward the electrochemical corrosion compared to the NSPI. Furthermore, we tried to measure the data of the NSPI-5%-coated CRS but failed, which might be caused from being over the detected limitation in our measuring condition. The Tafel plots for (a) uncoated, (b) NSPI-coated, (c) NSPI-0.5%-coated, (d) NSPI-1%-coated, (e) NSPI-3%-coated CRS are shown in Figure 5. Figure 5 shows novel advanced anticorrosive properties for NSPI and a series of PCN materials compared to bare CRS. The corrosion inhibition increased with the clay loading, indicating the inorganic clay with a platelike shape effectively increased the length of the diffusion pathways for oxygen and water as well as a decrease in the permeability of the coating.[33–34] This was further evidenced by the studies of the O_2 and H_2O molecular barrier effect as discussed in the following section.

Oxygen and water-vapor permeability of membranes

The oxygen permeability properties of the polyimide–clay nanocomposite materials were studied by a gas permeability analyzer with $\sim$ 55-μm membranes. As shown in Figure 6, the oxygen permeability properties of as-prepared PCN membranes were found to decrease gradually as the clay loading increased, indicating that the gas barrier properties of PCN materials were promoted by the dispersing of clay platelets. For the water-vapor permeability studies, we also found that the incorporation of clay platelets into NSPI matrix resulted in a decrease of H_2O vapor permeability. For example, the PCN membrane at low clay loading (e.g., 1 wt %) shows about 68 and 53% reduction of O_2 and H_2O permeability, respectively, compared to NSPI membrane.

Optical clarity of membranes

Figure 7 (a–e) shows the UV–visible transmission spectra of pure NSPI and PCN materials with 0.5–5 wt % MMT. These membranes had a thickness of $\sim$ 55 μm. The spectra of NSPI-0.5% and NSPI-1% in the visible regions (400–700 nm) were slightly affected by

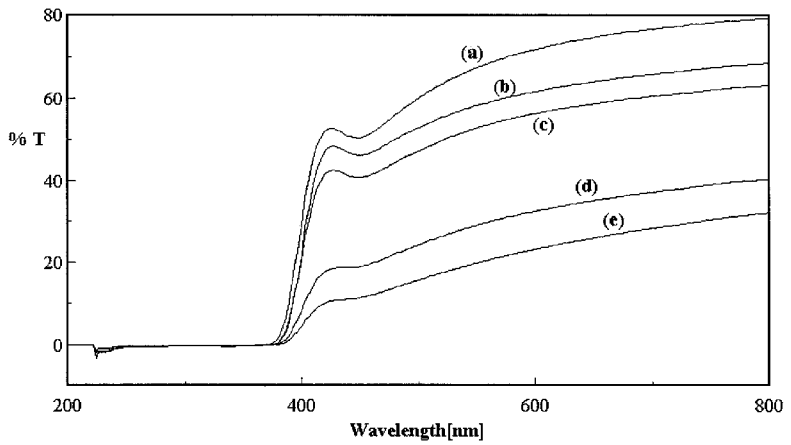

Figure 7 UV–visible transmission spectra of (a) NSPI, (b) NSPI-0.5%, (c) NSPI-1%, (d) NSPI-3% (e) NSPI-5%.

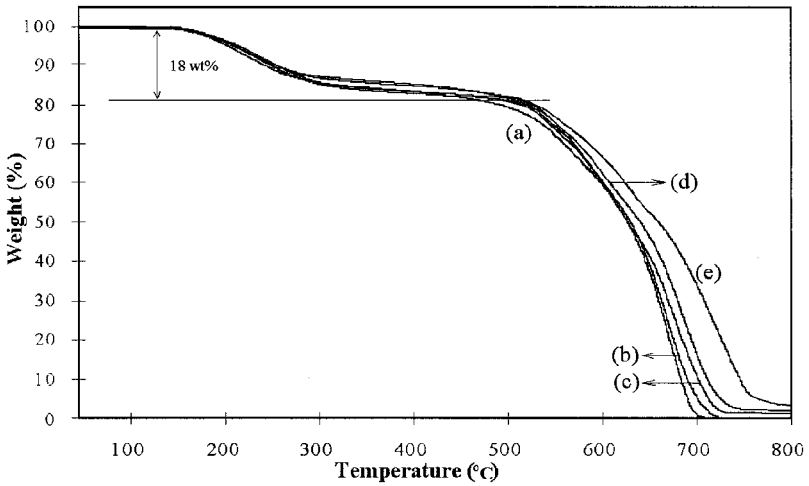

Figure 8 TGA curves of NSPI–clay nanocomposite materials: (a) NSPI, (b) NSPI-0.5%, (c) NSPI-1%, (d) NSPI-3%, (e) NSPI-5%.

the presence of the clay and retained the high transparency, indicating that exfoliated nanocomposite materials might exist at low clay contents. Furthermore, NSPI-3% had a much lower transparency than NSPI-0.5% or NSPI-1%, and very close to NSPI-5%. This result suggested that NSPI-3% might have mixed morphology similar to NSPI-5%. A close look at XRD (Fig. 3) suggested a broad peak around 5°, which was also evidence for the mixed morphology. The spectra of NSPI-5% exhibited low transparency reflected primarily in intercalated nanocomposite materials. There was strong scattering and/or absorption resulting in very low transmission of the UV light.

Thermal properties

Figure 8 showed typical TGA thermograms of weight loss as a function of temperature for NSPI and the PCN membranes prepared in an oven at 100°C for 8 h as measured under an air atmosphere. The TGA curves of NSPI and PCN membranes, two major weight losses, were observed in the range of ~ 150–300°C and at ~ 520°C for the NSPI membrane. The major weight loss at ~ 500–750°C was attributed to the structural decomposition of the polymer. The weight loss at ~ 150–300°C was assigned to the evaporation of the NMP solvent (boiling point = 202°C). The amount of NMP existing in the NSPI membrane estimated from the TGA thermogram was to be ~ 18 wt %; this value was similar to those obtained from the NMP-containing polyaniline membrane reported by Wei et al.[35] Furthermore, the thermal decomposition of those soluble PCN membranes shifted slightly toward the higher temperature range than that of NSPI, as shown in Figure 8(b–e). The char yield also increased along with the clay loading as listed in Table

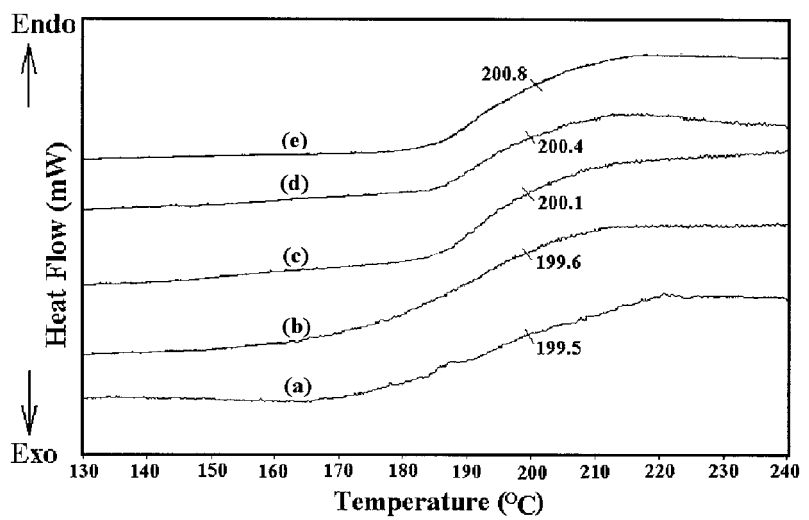

Figure 9 DSC curves of NSPI and a series of soluble PCN materials: (a) NSPI, (b) NSPI-0.5%, (c) NSPI-1%, (d) NSPI-3%, (e) NSPI-5%.

I. Thermal stability was slightly enhanced for the polyimide–clay nanocomposite material prepared by solution dispersion technique using the same molecular weight of NSPI. Figure 9 showed the DSC traces of the NSPI and PCN membranes. NSPI exhibited a shift of baseline near 199.5°C, corresponding to the T_g of NSPI. All the PCN materials were shown to have nearly same T_g compared to pure NSPI. This implied that the segmental motion behaviors of the polymer chains in these PCN materials prepared by solution dispersion were similar to the bulk NSPI.

CONCLUSION

PCN materials, in the form of coating, with low clay loading on CRS were found much superior in anticorrosion over those of NSPI based on a series of electrochemical measurements of corrosion potential, polarization resistance, and corrosion current in 5 wt % aqueous NaCl electrolyte. Therefore, the structurally modified soluble polyimide–clay nanocomposite materials might have significant potential for anticorrosion application. Effects of the material composition on the molecular barrier, optical clarity, and thermal properties of NSPI along with PCN materials, in the form of membrane, were also studied by molecular permeability analyses, UV–visible transmission spectra, TGA, and DSC, respectively. The incorporation of clay platelets into NSPI membrane resulted in an enhancement of O_2 and H_2O molecular permeability. Higher clay loading in NSPI membrane led to a significant decrease of optical clarity based on the UV–visible transmission spectra studies. Dispersed MMT clay platelets into NSPI matrix were found to slightly increase the thermal stability such as the enhancement of thermal decomposition temperature (T_d) and char yield of NSPI based on the TGA studies.

The financial support of this research by the NSC (90-2113M-033-010) is gratefully acknowledged.

References

1. Feld, W. A.; Ramalingam, B.; Harris, F. W. J Polym Sci, Polym Chem Ed 1983, 21, 319.
2. Imai, Y.; Maldar, N. N.; Kakimoto, M. J Polym Sci, Part A: Polym Chem 1984, 22, 2189.
3. Giesa, R.; Keller, U.; Schmidt, H. W. ACS Polym Prepr 1992, 33 (1), 396.
4. Jadhav, T. Y.; Preston, J.; Krigbaum, W. R. J Polym Sci, Part A: Polym Chem 1989, 27, 1175.
5. Liaw, D.-J.; Liaw, B.-Y.; Jeng, M.-Q. Polymer 1998, 39, 1597.
6. Lin, S.; Li, H. F.; Cheng, S. Z. D.; Harris, F. W. Macromolecules 1998, 31, 2080.
7. Yi, M. H.; Huang, W.; Choi, K. Y. Macromolecules 1997, 30, 5606.
8. Akutsu, F.; Inoki, M.; Araki, K.; Yasashima, Y.; Naruchi, K.; Miura, M. Polym J 1997, 29, 529.
9. Usuki, A.; Kawasumi, M.; Kojima, Y.; Okada, A.; Karauchi, T.; Kamigaito, O. J Mater Res 1993, 8, 1774.
10. Lan, T.; Kaviratna, P. D.; Pinnavaia, T. J. Chem Mater 1994, 6, 573.
11. Tyan, H.-L.; Liu, Y.-C.; Wei, K.-H. Chem Mater 1999, 11, 1942.
12. Wang, Z.; Pinnavaia, T. J. Chem Mater 1998, 10, 3769.
13. Gilman, J. W.; Jackson, C. L.; Morgan, A. B.; Hayyis, R., Jr.; Manias, E.; Giannelis, E. P.; Wuthenow, M.; Hilton, D.; Philips, S. H. Chem Mater 2000, 12, 1866.
14. Tyan, H.-L.; Liu, Y.-C.; Wei, K.-H. Chem Mater 1999, 11, 1942.
15. Morgam, A. B.; Gilman, J W.; Jackson, C. L. Macromolecules 2001, 34, 2735.
16. Agag, T.; Koga, T.; Takeichi, T. Polymer 2001, 42, 3399.
17. Gu, A.; Kuo, S.-W.; Chang, F.-C. J Appl Polym Sci 2001, 79, 1902.
18. Huang, J.-C.; Zhu, Z.-K.; Yin, J.; Qian, X.-F.; Sun, Y.-Y. Polymer 2001, 42, 873.
19. Zhu, Z.-K.; Yang, Y.; Yin, J.; Wang, X.-Y.; Ke, Y.-C.; Qi, Z.-N. J Appl Polym Sci 1999, 73, 2063.
20. Hsiao, S.-H.; Liou, G.-S.; Chang, L.-M. J Appl Polym Sci 2001, Vol. 80 2067.
21. Huang, J.-C.; Zhu, Z.-K.; Ma, X.-D.; Qian, X.-F.; Yin, J J Mater Sci 2001, 36, 871.
22. Yang, Y.; Zhu, Z.-K.; Yin, J; Wang, X.-Y.; Qi, Z.-E. Polymer 1999, 40, 4407.
23. Deberry, D. W. J Electrochem Soc 1985, 132, 1027.
24. Wessling, B. Synth Met 1991, 907, 1057.
25. Elsenbaumer, R. L.; Lu, W. K.; Wessling, B. International Conference of Synthetic Metals; Seoul, Korea, Abstract No. APL-(POL) 1–2, 1994.
26. Wrobleski, D. A.; Benicewicz, B. C.; Thompson, K. G.; Byran, C. J Polym Prepr (Am Chem Soc, Div Polym Chem) 1994, 35 (1), 265.
27. Wessling, B. Adv Mater 1994, 6, 226.
28. Wei, Y.; Wang, J.; Jia, X.; Yeh, J.-M.; Spellane, P. Polymer 1995, 36, 4535.
29. Yeh, J.-M.; Liou, S.-J.; Lai, C.-Y.; Wu, P.-C.; Tsai, T.-Y. Chem Mater 2001, 13(3), 1131.
30. Yeh, J.-M.; Chen, C.-L.; Chen, Y.-C.; Ma, C.-Y.; Lee, K.-R.; Wei, Y.; Li, S. Polymer 2002, 43, 2729.
31. Yeh, J.-M.; Liou, S.-J.; Lin, C.-Y.; Cheng, C.-Y.; Chang, Y.-W.; Lee, K.-R. Chem Mater 2002, 14(1), 154.
32. Chern, Y.-T.; Shiue, H.-C. Macromolecules 1997, 30, 4646.
33. Li, P.; Tan, T. C.; Lee, J. Y. Synth Met 1997, 88, 237.
34. Yano, K.; Usuki, A.; Okada, A.; Kurauchi, T.; Kamigaito, O. J Polym Sci, Polym Chem Ed 1993, 31, 2493.
35. Wei, Y.; Jang, G.-W.; Hsueh, K.-F.; Scherr, E. M.; MacDiarmid, A. G.; Epstein, A. J. Polymer 1992, 33 (2), 314.